

Excitation of whispering gallery magnons in a magnetic vortex

Schultheiss, K.; Verba, R.; Wehrmann, F.; Wagner, K.; Körber, L.; Hula, T.; Hache, T.; Kákay, A.; Awad, A. A.; Tiberkevich, V.; Slavin, A. N.; Fassbender, J.; Schultheiss, H.;

Originally published:

March 2019

Physical Review Letters 122(2019), 097202

DOI: <https://doi.org/10.1103/PhysRevLett.122.097202>

Perma-Link to Publication Repository of HZDR:

<https://www.hzdr.de/publications/Publ-28116>

Release of the secondary publication
on the basis of the German Copyright Law § 38 Section 4.

Excitation of whispering gallery magnons in a magnetic vortex

K. Schultheiss,¹ R. Verba,² F. Wehrmann,¹ K. Wagner,^{1,3} L. Körber,^{1,3} T. Hula,^{1,4} T. Hache,^{1,5} A. Kákay,¹ A.A. Awad,⁶ V. Tiberkevich,⁷ A.N. Slavin,⁷ J. Fassbender,^{1,3} and H. Schultheiss^{1,3}

¹*Helmholtz-Zentrum Dresden-Rossendorf, Institute of Ion Beam Physics and Materials Research, Bautzner Landstraße 400, 01328 Dresden, Germany*

²*Institute of Magnetism, National Academy of Sciences of Ukraine, Kyiv 03680, Ukraine*

³*Technische Universität Dresden, 01062 Dresden, Germany*

⁴*Westfälische Hochschule Zwickau, 08056 Zwickau, Germany*

⁵*Institut für Physik, Technische Universität Chemnitz, 09107 Chemnitz, Germany*

⁶*Department of Physics, University of Gothenburg, 412 96 Gothenburg, Sweden*

⁷*Department of Physics, Oakland University, Rochester, MI 48309, USA*

(Dated: 27 August 2018)

We present the generation of whispering gallery magnons with unprecedented high wave vectors via nonlinear 3-magnon scattering in a μm -sized magnetic vortex state disc. These modes exhibit a strong localisation at the perimeter of the disc and practically zero amplitude in an extended area around the vortex core. They originate from the splitting of the fundamental radial magnon modes, which can be resonantly excited in a vortex texture by an out-of-plane microwave field. We shed light on the basics of this non-linear scattering mechanism from experimental and theoretical point of view. Using Brillouin light scattering (BLS) microscopy, we investigated the frequency and power dependence of the 3-magnon splitting. The spatially resolved mode profiles give evidence for the localisation at the boundaries of the disc and allow for a direct determination of the modes wavenumber.

One of the most fascinating topics in current quantum physics are hybridized systems, in which different quantum resonators are strongly coupled. Prominent examples are circular cavities that allow the coupling of optical whispering gallery modes^{1–5} to microwave cavities⁶ or magnetic resonances^{7–10}. Whispering gallery modes play a special role in this endeavour because of their high quality factor and strong localisation, which ultimately increases the overlap of the wave functions of quantum particles in hybridized systems. In optomagnonics the hybridisation with magnons, the collective quantum excitations of the electron spins in a magnetically ordered material, is of particular interest because magnons can take over two functionalities: due to their collective nature they are robust and can serve as a quantum memory¹¹ and, moreover, they can act as a wavelength converter between microwave and terahertz photons⁹. However, the observation of whispering gallery magnons has not yet been achieved due to the lack of efficient excitation schemes for magnons with large wave vectors in a circular geometry. To tackle this problem, we studied nonlinear 3-magnon scattering^{12–15} as a means to generate whispering gallery magnons. This Letter discusses the basics of this nonlinear mechanism in a confined, circular geometry from experimental and theoretical point of view.

Whispering gallery magnons are eigenmodes in systems with rotational symmetry. This not only applies to the geometry of the magnetic element but also to the magnetisation texture therein. For that reason, we study a $\text{Ni}_{81}\text{Fe}_{19}$ disc that inherently exhibits a magnetic vortex structure^{16–20}. The arrows in Fig. 1(a) schematically depict the generic features of such a vortex state: the magnetic moments curl in plane along circular lines around the vortex core, a nanoscopic region in the center of the

disc where the magnetisation tilts out of plane. According to this rotational symmetry, the magnon eigenmodes in a vortex are characterised by mode numbers (n, m) , with $n = 0, 1, 2, \dots$ counting the number of nodes across the disc radius and $m = 0, \pm 1, \pm 2, \dots$ counting the number of nodes in azimuthal direction over half the disc^{21,22}.

Other than commonly known waves, like sound, water, or electromagnetic waves, magnons exhibit a strongly anisotropic dispersion relation in in-plane magnetised thin films²¹. In a vortex, this results in increasing (decreasing) mode energies for increasing n (m) as shown by our analytic calculations in Fig. 1(b) (see supplementary material for details). The four exemplary intensity profiles for the eigenmodes $(0, 0)$, $(0, 10)$, $(0, 20)$, and $(0, 30)$, that are shown in Fig. 1(c), reveal the character of whispering gallery magnons: the larger m , the more the magnon intensity is pushed toward the perimeter of the disc. This can be understood intuitively by the reduction of exchange energy: Leaving an extended area around the vortex core with zero amplitude avoids a strong tilt of neighbouring spins close to the vortex core and, therefore, reduces the total energy.

Even though magnon spectra in magnetic vortices have been intensively studied in the past^{20,22–24}, magnons with large azimuthal wave vectors have not yet been measured experimentally and were only observed in micromagnetic simulations²⁵. The challenge to generate such magnons and, thereby, to reach out to whispering gallery magnons is finding an efficient excitation mechanism. Here, we tackle this problem via nonlinear 3-magnon scattering. In this process, one magnon splits in two magnons under conservation of energy and momentum. The rotational symmetry of the vortex texture implies specific selection rules for the scattering process which we will describe in

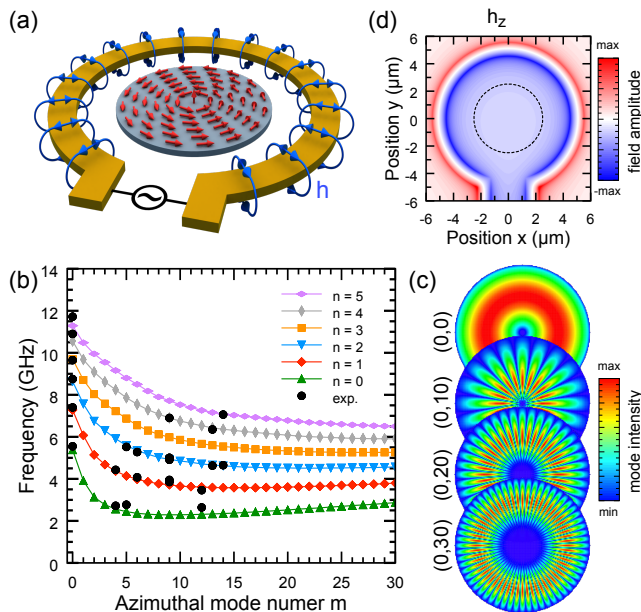


FIG. 1. (color online) (a) A $\text{Ni}_{81}\text{Fe}_{19}$ disc with 50 nm thickness and $5.1\ \mu\text{m}$ diameter is patterned inside an Ω -shaped antenna. Red arrows depict the magnetisation configuration of the magnetic vortex structure and the blue lines represent the dynamic magnetic field generated by the loop shaped microwave antenna. (b) Analytical calculation of the magnon mode frequencies as a function of the radial and azimuthal mode numbers n, m (see supplementary material). Black dots show experimental results. (c) Four exemplary mode profiles resulting from analytical calculations. The larger m , the more pronounced the character of the whispering gallery magnons is revealed. (d) COMSOL simulation of the z -component of exciting magnetic field \mathbf{h} generated by the Ω -shaped antenna. The dashed circle indicates the size and position of the disc.

context with the experimental data.

In order to selectively excite magnetisation dynamics, we apply microwave currents to an Ω -shaped antenna that encloses the vortex. Inside the Ω loop, a spatially uniform magnetic field is generated that is oriented perpendicularly to the disc as shown in Fig. 1(d). The rotational symmetry of this magnetic field prohibits direct coupling to magnons with $m \neq 0$. However, because of the small diameter of the antenna, strong magnetic fields can be generated so that these magnons can be indirectly excited in the nonlinear regime via multi-magnon scattering processes.

We track these nonlinear processes by measuring magnon spectra as a function of the applied microwave frequency using Brillouin light scattering (BLS) microscopy²⁶. We would like to emphasise that even though the system is driven with one particular microwave frequency, the BLS technique allows us to detect the dynamic magnetic response in a broad frequency range. In Fig. 2(a)-(c) we plot the BLS spectra measured between 2 and 11 GHz (y -axis) for each excita-

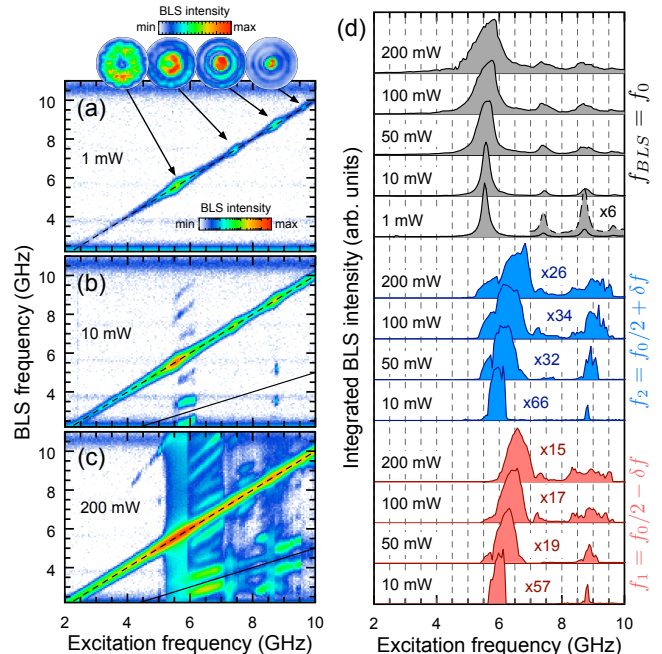


FIG. 2. (color online) (a)-(c) BLS spectra for excitation frequencies f_0 between 2 and 10 GHz and excitation powers of 1, 10, and 200 mW, respectively. The diagonal dashed lines indicate the directly excited magnetic oscillations at $f_{\text{BLS}} = f_0$. At 10 and 200 mW, off-diagonal signals associated with multi-magnon scattering processes are detected. (d) Black data show the BLS intensity integrated in 800-MHz wide windows around the direct excitation for 1, 10, 50, 100, and 200 mW (bottom to top). At 1 mW, the intensity integrated for excitation frequencies between 7 and 10 GHz was multiplied by a factor of six to better visualise the resonances of the higher order radial modes. Blue (red) data show the intensities of the split modes integrated in 1.4-GHz wide windows around $f_1 = f_0/2 + \delta f$ ($f_2 = f_0/2 - \delta f$) with $\delta f = 800$ MHz.

tion frequency (x -axis) at microwave powers of 1, 10, and 200 mW. The magnon intensity is encoded using the same logarithmic scale shown as an inset in Fig. 2(a).

At the lowest microwave power of 1 mW [Fig. 2(a)], magnons are excited in the linear regime, which is corroborated by the fact that magnons are only observed at the BLS frequency that matches the applied microwave frequency $f_{\text{BLS}} = f_0$. Hence, the measured intensities strictly follow the diagonal, dashed line. Four distinct resonances emerge at 5.55, 7.40, 8.75, and 9.65 GHz, which we identify as the well known first four radial modes^{22,27} by spatially-resolved BLS microscopy [insets in Fig. 2(a)].

At a power of 10 mW [Fig. 2(b)], the excitation field is strong enough to generate magnons in the nonlinear regime. Hence, we observe strong off-diagonal signals that appear at BLS frequencies symmetrically spaced around half the excitation frequency $f_0/2$ (straight line with slope 0.5). These satellite peaks are the result of 3-magnon splitting processes. In order to conserve en-

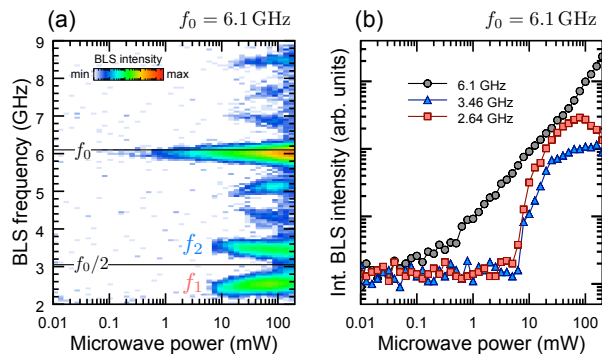


FIG. 3. (color online) (a) Power dependence of the BLS spectra excited at $f_0 = 6.1$ GHz. (b) BLS intensity integrated in 800-MHz wide frequency windows around the BLS frequencies $f_0 = 6.1$ GHz, $f_1 = 2.64$ GHz, and $f_2 = 3.46$ GHz as a function of the microwave power. In the double-logarithmic plot, the direct excitation at 6.1 GHz follows a linear trend, whereas the split modes at 3.46 and 2.64 GHz show a clear threshold behaviour.

ergy the initial magnon with frequency f_0 splits in two magnons with frequencies $f_1 = f_0/2 - \delta f$ and $f_2 = f_0/2 + \delta f$. Moreover, the rotational symmetry of the vortex requires conservation of the momentum component in azimuthal direction. For an initial magnon with $m = 0$ this implies that the split modes have azimuthal mode numbers with the same modulus but opposite sign: $m_1 = -m_2$. Our analytic calculations further show that the split modes must not share the same radial index, *i.e.*, $n_1 \neq n_2$ (see supplementary material). All three selection rules drastically restrict the possible scattering channels within the discrete eigenmode spectrum of the vortex [see Fig. 1(b)].

At the maximum applied microwave power of 200 mW, the number of off-diagonal signals increases further [Fig. 2(c)]. Especially, for excitation frequencies between 6 and 7 GHz, we do not just measure two satellite peaks with frequencies f_1 and f_2 but a total number of ten additional modes. Their presence is attributed to avalanche processes of higher order multi-magnon scattering. Their frequencies are given by combinations of the three initial magnons, *e.g.*, $2f_1$, $2f_2$, $f_0 + f_1$. Furthermore, the significant line broadening of the directly excited mode and of the split modes in the frequency range between 5.3 and 5.9 GHz can be attributed to 4-magnon scattering²⁸. However, this article solely focusses on the study of the initial 3-magnon scattering processes which dominate in intensity due to the lower threshold compared to 4-magnon scattering.

To better illustrate the power dependence of the observed modes, we plot the BLS intensity integrated over different frequency windows as a function of the excitation frequency in Fig. 2(d). The black data resembles the BLS intensity of the direct excitation. With increasing power the initially sharp resonances become broader

and show the characteristic nonlinear foldover to higher frequencies^{29,30}. The red and blue data in Fig. 2(d) show the intensities of the split modes below (red data) and above $f_0/2$ (blue data), which overall broaden in range and shift to higher frequencies with increasing power.

To further elucidate the threshold character of the 3-magnon splitting, we plot a more detailed power dependence of the magnon intensities in Fig. 3(a) for $f_0 = 6.1$ GHz. While the mode at 6.1 GHz can be observed over a large power range, it is evident that the split modes f_1 and f_2 only appear above a certain threshold power. Furthermore, we observe a pronounced frequency shift of these two split modes with increasing microwave power. For a quantitative comparison, we integrate the BLS intensity in narrow frequency windows around the directly and indirectly excited modes, respectively, and plot them in Fig. 3(b). The double logarithmic scale reveals the linear growth of the direct excitation at 6.1 GHz starting at 0.1 mW. However, the intensities of the satellite peaks around $f_1 = 2.65$ GHz and $f_2 = 3.48$ GHz abruptly increase above 10 mW which demonstrates the threshold character of the splitting process.

In order to reveal the spatial structure of the modes that are generated via 3-magnon scattering, we simultaneously mapped the profiles of the directly excited mode and the split modes [Fig. 4(c)-(g)]. Additionally, we compare the experimental results for the mode with highest intensity at 6.1 GHz with micromagnetic simulations³² [Fig. 4(b)]. The first thing to realise is that all of the split modes show a clear azimuthal character and confirm the analytical calculations and the selection rules imposed by the rotational symmetry: pure radial modes with $(n, 0)$ split in modes with $m_1 = -m_2$ and $n_1 \neq n_2$. As far as possible, we label the modes according to their radial and azimuthal mode numbers (n, m) . We resolve azimuthal mode numbers up to 14, to our knowledge the first time to observe vortex modes with such high m . For higher n , an unambiguous identification of the modes was not possible due to limited spatial resolution. However, the radial mode number can still be retrieved by comparing the measured frequencies to the analytic calculations in Fig. 1(b). We counted the azimuthal mode numbers and plotted the measured frequencies as black dots in the calculated spectrum. From this comparison we then determined the radial mode numbers (red labels in Fig. 4).

In Fig. 4(b), the micromagnetic simulation for excitation at 6.1 GHz reveals the splitting into magnons with the same mode numbers as in the experiment, however, with slightly different frequencies of the split modes. This frequency shift may be attributed to variations in the strength and symmetry of the exciting magnetic field or the material parameters. For further details please see supplementary material.

Note that we only measure stationary mode profiles which implies that, essentially, all split modes are a superposition of modes counter propagating in azimuthal direction. Therefore, we conclude that the two splitting processes $(n_0, 0) \rightarrow (n_1, m) + (n_2, -m)$ and $(n_0, 0) \rightarrow$

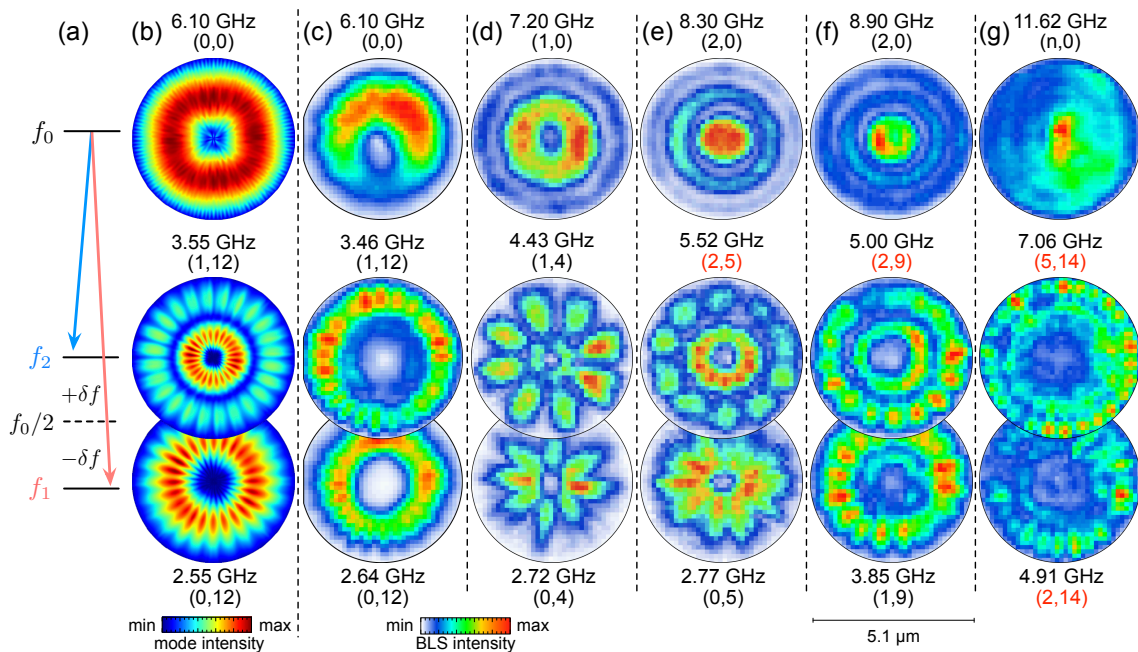


FIG. 4. (color online) (a) Energy levels for 3-magnon splitting. (b) Micromagnetic simulation of the 3-magnon splitting for the excitation frequency of 6.1 GHz. (c)-(g) Spatial intensity distributions of the direct excitation (upper line) as well as the split modes (middle and bottom line) for various excitation frequencies. Each magnon mode has been identified regarding its radial and azimuthal order (n, m) . Numbers in red are derived by comparing the experimentally detected magnon frequency to analytical calculations (Fig. 1b).

$(n_1, -m) + (n_2, m)$ occur with equal probability.

It is remarkable, that the higher m for a given n , the stronger the mode is localised at the outer circumference of the disc, resembling intensity distributions of optical whispering gallery modes³¹. The most beautiful example in our dataset is the intensity distribution of the split mode $(0, 12)$ at the excitation frequency 6.1 GHz shown in Fig. 3(c). It exhibits a distinct area with zero intensity in its center, similar to higher order optical whispering gallery modes.

In summary, we shed light on the nonlinear conversion of magnons in a confined system with rotational symmetry by analysing their spectral and spatial characteristics. We showed how this mechanism can be utilised to generate magnons with unprecedented high azimuthal wave vectors and localisation at the discs perimeter, which resembles the character of whispering gallery modes. The underlying 3-magnon scattering processes are highly tunable regarding the frequency and spatial distribution of the split modes. We believe that this advanced control of the generation of whispering gallery magnons is a missing link towards the realisation of an efficient hybridisation of magnons and other quantum particles as found in circular optical cavities and mechanical quantum resonators.

The authors acknowledge fruitful discussions with S.V. Kusminskiy. Financial support by the Deutsche Forschungsgemeinschaft is gratefully acknowledged within program SCHU2922/1-1. K.S. acknowledges funding within the Helmholtz Postdoc Programme.

Samples were fabricated at the Nanofabrication Facilities (NanoFaRo) at the Institute of Ion Beam Physics and Materials Research at HZDR. We thank B. Scheumann for film deposition and L. Bischoff for the thickness measurement.

- ¹Mie, G. Beiträge zur Optik trüber Medien, speziell kolloidaler Metallösungen. *Ann. Phys.* **25**, 377-445 (1908).
- ²Debye, P. Der Lichtdruck auf Kugeln von beliebigem Material. *Ann. Phys.* **30**, 57136 (1909).
- ³Rayleigh, L. Further applications of Bessel's functions of high order to the whispering gallery and allied problems. *Phil. Mag.* **27**, 100 (1914).
- ⁴Oraevsky, A. N. Whispering-gallery waves. *Quant. Electron.* **32**, 377-400 (2002).
- ⁵Vahala, K. J. Optical microcavities. *Nature* **424**, 839-846 (2003).
- ⁶Tabuchi, Y. et al. Hybridizing Ferromagnetic Magnons and Microwave Photons in the Quantum Limit. *Phys. Rev. Lett.* **113**, 083603 (2014).
- ⁷Osada, A. Cavity Optomagnonics with Spin-Orbit Coupled Photons. *Phys. Rev. Lett.* **116**, 223601 (2016).
- ⁸Haigh, J. A., Nunnenkamp, A., Ramsay, A. J., & Ferguson, A. J., *Phys. Rev. Lett.* **117**, 133602 (2016).
- ⁹Kusminskiy, S. V., Tang, H. X., & Marquardt, F., Coupled spin-light dynamics in cavity optomagnonics. *Phys. Rev. Appl.* **9**, 033821 (2016).
- ¹⁰Graf, J., Pfeifer, H., Marquardt, F., & Kusminskiy, S. V. Cavity optomagnonics with magnetic textures: coupling a magnetic vortex to light. arXiv:1806.06727v1 (2018).
- ¹¹Zhang X., Y. et al. Magnon dark modes and gradient memory. *Nat. Comm.* **6**, 8914 (2015).
- ¹²Suhl, H. The theory of ferromagnetic resonance at high signal powers. *J. Phys. Chem. Solids.* **1**, 209 (1957).
- ¹³Ordóñez-Romero, C. et al. Three-magnon splitting and conflu-

- ence processes for spin-wave excitations in yttrium iron garnet films: Wave vector selective Brillouin light scattering measurements and analysis. *Phys. Rev. B* **79**, 144428 (2009).
- ¹⁴Schultheiss, H. *et al.* Direct Current Control of Three Magnon Scattering Processes in Spin-Valve Nanocontacts. *Phys. Rev. Lett.* **103**, 157202 (2009).
- ¹⁵Camley, R.E. Three-magnon processes in magnetic nanoelements: Quantization and localized mode effects. *Phys. Rev. B* **89**, 214402 (2014).
- ¹⁶Shinjo, T., Okuno, T., Hassdorf, R., Shigeto, K., & Ono, T., Magnetic vortex core observation in circular dots of permalloy. *Science* **289**, 930 (2000).
- ¹⁷Novosad, V. *et al.* Spin excitations of magnetic vortices in ferromagnetic nanodots. *Phys. Rev. B* **66**, 052407 (2002).
- ¹⁸Guslienko, K.Y. & Novosad, V. Vortex state stability in soft magnetic cylindrical nanodots. *J. Appl. Phys.* **96**, 4451 (2004).
- ¹⁹Novosad, V., *et al.* Magnetic vortex resonance in patterned ferromagnetic dots. *Phys. Rev. B* **72**, 024455 (2005).
- ²⁰Guslienko, K. Y., Slavin, A. N., Tiberkevich, V., & Kim, S.-K. Dynamic origin of azimuthal modes splitting in vortex-state magnetic dots. *Phys. Rev. Lett.* **101**, 247203 (2008).
- ²¹Kalinikos, B. A. & Slavin, A. N. The dipole-exchange spin wave spectrum for anisotropic ferromagnetic films with mixed exchange boundary conditions. *J. Phys. C* **19**, 7013 (1986).
- ²²Buess, M. *et al.* Fourier transform imaging of spin vortex eigenmodes. *Phys. Rev. Lett.* **93**, 077207 (2004).
- ²³Zivieri, R. & Nizzoli, F. Theory of spin modes in vortex-state ferromagnetic cylindrical dots. *Phys. Rev. B* **71** (2005).
- ²⁴Awad, A. *et al.* Spin excitation frequencies in magnetostatically coupled arrays of vortex state circular Permalloy dots. *Appl. Phys. Lett.* **97**, 132501 (2010).
- ²⁵Taurel, B. *et al.* Complete mapping of the spin-wave spectrum in a vortex-state nanodisk. *Phys. Rev. B* **93**, 184427 (2016).
- ²⁶Sebastian, T., Schultheiss, K., Obry, B., Hillebrands, B. & Schultheiss, H. Micro-focused Brillouin light scattering: imaging spin waves at the nanoscale. *Front. Phys.* **3**, 35 (2015).
- ²⁷Vogt, K. *et al.* Optical detection of vortex spin-wave eigenmodes in microstructured ferromagnetic disks. *Phys. Rev. B* **84**, 174401 (2011).
- ²⁸Schultheiss, H., Vogt, K. Hillebrands, B. Direct observation of nonlinear four-magnon scattering in spin-wave microconduits. *Phys. Rev. B* **86**, 054414 (2012).
- ²⁹Suhl, H. Foldover effects caused by spin wave interactions in ferromagnetic resonance. *J. Appl. Phys.*, **31**, 935 (1960).
- ³⁰Janantha, P. A. P., Kalinikos, B., and Wu, M. Foldover of nonlinear eigenmodes in magnetic thin film based feedback rings. *Phys. Rev. B* **95**, 064422 (2017).
- ³¹Yang, J. J., Huang, M., Yu, J., & Lan, Y. Z. Surface whispering-gallery mode. *Europhys. Lett.* **96**, 57003 (2011).
- ³²Vansteenkiste, A. *et al.* The design and verification of MuMax3. *AIP Adv.* **4**, 107133 (2014).